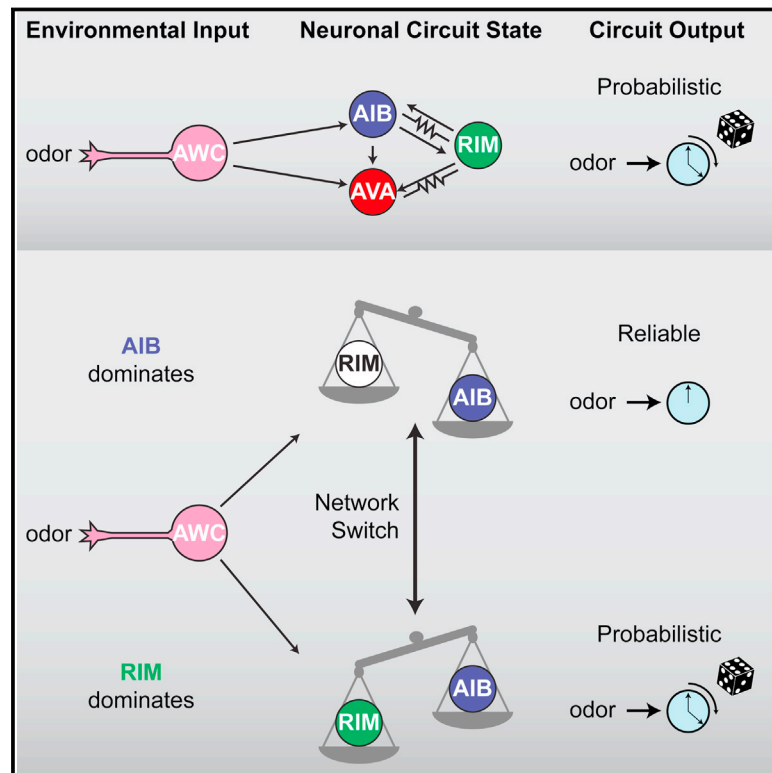


# Feedback from Network States Generates Variability in a Probabilistic Olfactory Circuit

## Graphical Abstract



## Authors

Andrew Gordus, Navin Pokala, ..., Steven W. Flavell, Cornelia I. Bargmann

## Correspondence

cori@rockefeller.edu

## In Brief

Even when a stimulus invariably activates a sensory neuron, the motor output/behavior is probabilistic because of variability in the network state of interneurons downstream of the sensory neuron. Manipulating the activity of these interneurons relative to one another can drive olfactory responses in *C. elegans* to be more deterministic.

## Highlights

- Interneurons in an olfactory circuit have variable responses to a fixed odor input
- Interneurons participate in collective network states that correlate with behavior
- Reliability of the AIB interneuron's odor response depends on the network activity state
- Chemical synapses from the RIM interneuron increase variability of the odor response



# Feedback from Network States Generates Variability in a Probabilistic Olfactory Circuit

Andrew Gordus,<sup>1</sup> Navin Pokala,<sup>1</sup> Sagi Levy,<sup>1</sup> Steven W. Flavell,<sup>1</sup> and Cornelia I. Bargmann<sup>1,\*</sup>

<sup>1</sup>Howard Hughes Medical Institute and Lulu and Anthony Wang Laboratory of Neural Circuits and Behavior, The Rockefeller University, New York, NY 10065, USA

\*Correspondence: [cori@rockefeller.edu](mailto:cori@rockefeller.edu)

<http://dx.doi.org/10.1016/j.cell.2015.02.018>

## SUMMARY

Variability is a prominent feature of behavior and is an active element of certain behavioral strategies. To understand how neuronal circuits control variability, we examined the propagation of sensory information in a chemotaxis circuit of *C. elegans* where discrete sensory inputs can drive a probabilistic behavioral response. Olfactory neurons respond to odor stimuli with rapid and reliable changes in activity, but downstream AIB interneurons respond with a probabilistic delay. The interneuron response to odor depends on the collective activity of multiple neurons—AIB, RIM, and AVA—when the odor stimulus arrives. Certain activity states of the network correlate with reliable responses to odor stimuli. Artificially generating these activity states by modifying neuronal activity increases the reliability of odor responses in interneurons and the reliability of the behavioral response to odor. The integration of sensory information with network states may represent a general mechanism for generating variability in behavior.

## INTRODUCTION

Variability is intrinsic to behavior. The behavioral response of individuals to a defined sensory stimulus varies from trial to trial, even when it is predictable on average. Although variability may limit task performance, both behavioral and theoretical analyses suggest that it can also be a creative element of behavioral strategies (Thrun, 1992; Hessler and Doupe, 1999; Ölveczky et al., 2005; Tumer and Brainard, 2007; Chaisanguanthum et al., 2014). In foraging animals, behavioral variation over short and long timescales allows efficient exploration of environments with unevenly distributed resources (Charnov, 1976; Humphries et al., 2010). In an analogous fashion, computer machine-learning algorithms use variability to escape local minima and reach global optima (Kirkpatrick et al., 1983; Mitsutake et al., 2013). Game-theoretical approaches suggest that variable strategies are often the best responses to unpredictable conditions, particularly in the presence of competitors or predictors (Harsanyi, 1973). At a neuronal level, intrinsically generated variability provides a substrate for reward learning, and increased variability has been linked to enhanced learning in motor tasks

(Ölveczky et al., 2005; Tumer and Brainard, 2007; Chaisanguanthum et al., 2014).

Trial-to-trial variability in responses to a sensory stimulus can result from several mechanisms. There is unavoidable noise in sensory systems operating near their detection or discrimination thresholds (Barlow et al., 1971; Lillywhite and Laughlin, 1979; Bialek, 1987). This stochastic noise decreases precision, but it can enhance sensitivity to weak signals (Benzi et al., 1981; Longtin et al., 1991). At subsequent levels, noise in synaptic transmission or cellular properties can alter signal propagation at any point between sensory and motor systems. Finally, the state of the neuronal network when a signal arrives can influence the network response, especially if its dynamics are highly sensitive to initial conditions (Rajan et al., 2010). However, it is challenging to ascribe single-trial variation to a precise source in complex systems in which the neuronal source of behavioral variation must be indirectly inferred from population measurements of neuronal activity.

The compact nervous system of the nematode worm *Caenorhabditis elegans*, which has only 302 neurons and about 7,000 connections (White et al., 1986), provides an opportunity to address the neuronal sources of behavioral variability. Variability is an explicit element of *C. elegans* behavioral strategies for locating attractants. As first described in bacteria, a biased random walk allows organisms to approach an attractant source by changing their turning rates on the basis of whether stimulus concentrations are increasing or decreasing (Berg and Brown, 1972). In this probabilistic behavior, the rate of turning is predictable, but individual reorientation events are not. *C. elegans* has probabilistic reversal (reorientation) responses to odors, tastes, and temperature associated with chemotaxis and thermotaxis behaviors (Pierce-Shimomura et al., 1999; Clark et al., 2007). The sensory neurons and circuits for these behaviors have been extensively characterized, but it is not known where in the circuit a decision is made to reorient movement.

*C. elegans* neurons fall into three computational levels: sensory neurons that gather information, motor neurons that synapse onto muscle, and extensively interconnected interneurons. *C. elegans* chemotaxis to attractive odors such as isoamyl alcohol (IAA) is initiated by two AWC olfactory neurons. Attractive odors decrease AWC calcium levels and suppress reversal behaviors as part of a biased random walk strategy, whereas odor removal increases AWC calcium and stimulates reversals (Chalasanani et al., 2007; Albrecht and Bargmann, 2011). The AWC calcium response, which is likely correlated

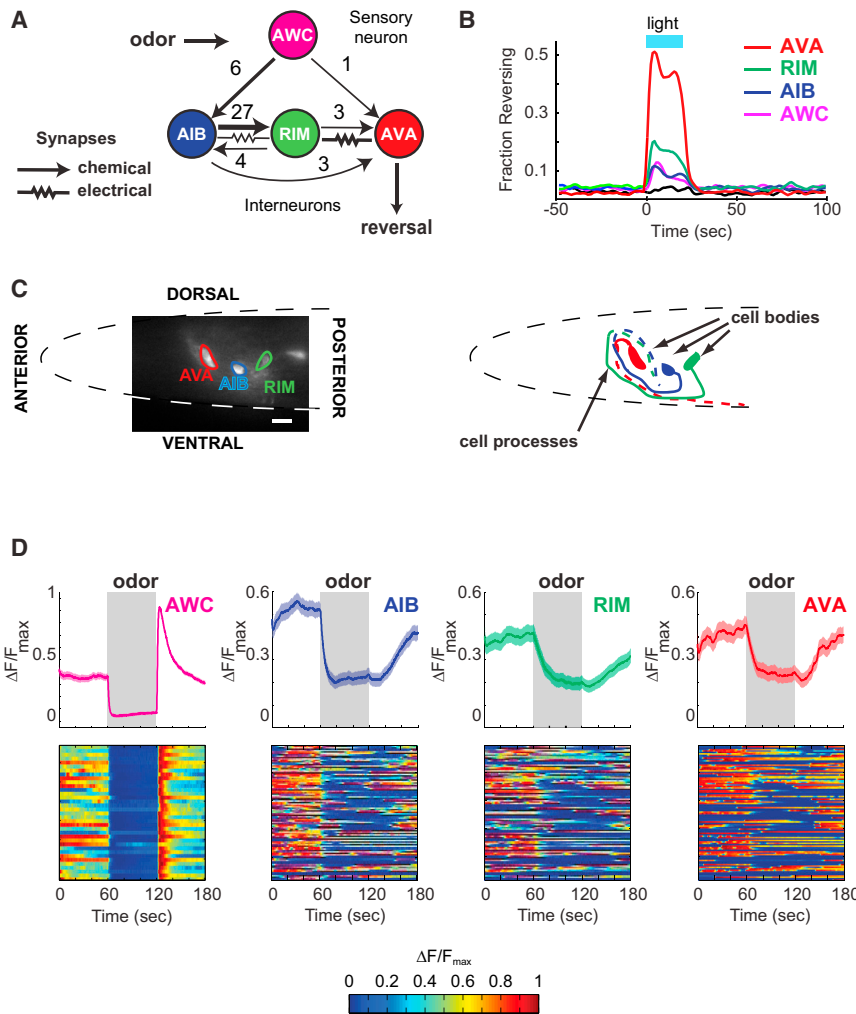


**Figure 1. Calcium Dynamics of AIB, RIM, and AVA Neurons in Response to Odor**

(A) Simplified wiring diagram showing AWC sensory neurons and three interneurons in a circuit linking AWC to reversal behavior, and the number of direct synapses between each pair of neurons (White et al., 1986). A more complete circuit appears in Figure 7.

(B) Light-induced reversal behaviors in wild-type animals expressing Channelrhodopsin2 (ChR2) in specific neurons, showing the instantaneous fraction of animals reversing; the total percentage of animals that respond is higher (Figure S1A). The low light levels used here (0.025 mW/mm<sup>2</sup>) did not activate the endogenous *C. elegans* light avoidance response (black line).

(C) Single frame showing AIB, RIM, and AVA neurons expressing GCaMP3 in an animal restrained in the microfluidic imaging chip, and schematic showing the head of the animal and location of neurons and processes. Dashed lines represent processes on the contralateral side of the head; the AIB, RIM, and AVA neurons from the contralateral side are not shown. Scale bar, 10 μm.

(D) Averaged calcium responses to a 1-min exposure to 92 μM IAA (top) and individual traces (bottom). AIB, RIM, and AVA were recorded simultaneously and aligned in the same order in each panel (n = 83); AWC was recorded independently (n = 35). Calcium dynamics were normalized to peak and trough values for each trace before averaging. Shaded area is SEM.

with depolarization, is highly reliable from trial to trial, even after dozens of odor presentations (Larsch et al., 2013). By contrast, the reversal response is probabilistic. Even under well-controlled conditions, animals may or may not reverse on individual trials, regardless of the strength of the AWC calcium response (Larsch et al., 2013). Most reversals rely upon the two AVA command interneurons, which synapse onto motor neurons that control the final common pathway for transitions from forward to backward movement (Chalfie et al., 1985). An increase in AVA calcium activity consistently correlates with the beginning of a reversal, and a decrease with its termination (Chronis et al., 2007; Ben Arous et al., 2010; Faumont et al., 2011). Thus, the variability in the behavioral response results from variable transmission of information from the AWC sensory neuron to AVA command neurons.

The *C. elegans* connectome provides a framework to examine the intermediate steps of information propagation at the single-neuron level. Here we show that the AIB and RIM interneurons that link AWC to AVA integrate sensory information with ongoing network states to produce neuronal and behavioral variability. We find that the instantaneous activity state of the integrating

network can predict its response to odor stimuli and that artificially generating certain activity states by modifying RIM activity can increase the reliability of AVA responses and behavior. Internal network states may serve as a source of

## RESULTS

### Odor-Evoked Calcium Responses in AIB, RIM, and AVA

Among several neuronal pathways connecting AWC to motor output, four pairs of neurons—AWC, AIB, RIM, and AVA—represent a starting point for defining a connectivity diagram for reversals (White et al., 1986; Figure 1A). The *C. elegans* wiring diagram predicts a single direct synaptic connection between AWC sensory neurons and AVA backward command neurons, but a much greater number of indirect connections. Most reversals initiated by AWC require the two AIB interneurons, which are major synaptic targets of AWC and many other sensory neurons (Gray et al., 2005; White et al., 1986). AIB has a few direct synapses onto AVA and a much stronger indirect connection to AVA through the two RIM interneurons, which are connected to both AIB and AVA by chemical and electrical synapses. RIM neurons also form neuromuscular junctions that affect head movements, which were not studied here.

AWC, AIB, and AVA stimulate odor-evoked and spontaneous reversals (Gray et al., 2005; Chalasani et al., 2007; Guo et al., 2009), but experiments conducted in different conditions and genetic backgrounds have led to ambiguous conclusions about whether RIM stimulates or inhibits reversals (Gray et al., 2005; Guo et al., 2009; Piggott et al., 2011). To clarify this relationship, we depolarized each neuron type individually in wild-type animals by cell-specific expression and activation of Channelrhodopsin2 (Nagel et al., 2005). Acute light stimulation of AWC, AIB, RIM, or AVA resulted in increased reversal behaviors (Figure 1B; Figure S1), suggesting that the net activity of each neuron promotes reversals.

To monitor information flow between these neurons, we imaged calcium in animals expressing the genetically encoded calcium indicator GCaMP3 (Tian et al., 2009) in AWC, AIB, RIM, and AVA individually and in combinations. Animals were restrained in a small microfluidic chamber that allowed precise delivery and removal of odor stimuli to the nose (Figures 1C and S1) (Chronis et al., 2007). AWC and AIB have previously been examined in this imaging system (Chalasani et al., 2007), but RIM and AVA have not. AWC responds to odor addition with an immediate reduction in calcium and to odor removal with a sharp calcium rise followed by a return to baseline levels (Figure 1D). AIB, RIM, and AVA responded to odor addition with a calcium decrease relative to the average baseline, and to odor removal with a slow return toward the baseline, without an overshoot (Figure 1D). The interneuron calcium responses appeared smaller in magnitude and slower than those of AWC neurons. We focused subsequent analysis on odor addition, in part because of its robustness and in part because the more complex response to odor removal is regulated by odor history as well as concentration (Chalasani et al., 2007).

### AIB, RIM, and AVA Have Distinct High and Low Activity States

Examination of individual traces revealed an unexpected feature of calcium signals in AIB, RIM, and AVA not visualized in the averages: the neurons appeared to switch between long-lasting high and low calcium states, spending little time at intermediate values (Figures 1D and 2A–2C). Furthermore, transitions between high and low states for all three neurons often occurred at the same time, both spontaneously in buffer (Figure 2A) and in response to odor stimuli (Figure 2C). Quantitative analysis confirmed that AIB, RIM, and AVA calcium signals had a bimodal distribution, with a strong bias toward distinct high and low states (Figure 2B). While *C. elegans* neurons lack classical sodium-based action potentials, they do have voltage-activated channels that can generate active properties such as bistability (Goodman et al., 1998; Mellem et al., 2008).

Calcium signals in *C. elegans* neurons are generally correlated with depolarization, but can vary between cellular compartments (Chalasani et al., 2007; Hendricks et al., 2012). The presynaptic calcium that drives neurotransmitter release is most relevant to neuronal function and can be observed directly by monitoring GCaMP signals in axons. Like somatic responses, calcium signals in the axons of AIB, RIM, and AVA neurons were bimodal, with long-lasting high and low states (Figure S2A). They began to rise or fall at the same time as somatic calcium signals, but

the response magnitude peaked more quickly in the axon, especially for RIM (Figure 2D). Odor-evoked activity in axons rose and fell with similar dynamics in AIB, RIM, and AVA (Figure 2D). Because of the proximity of AIB, RIM, and AVA axons, simultaneous imaging was only possible for cell bodies.

We defined distinct ON and OFF states for AIB, RIM, and AVA on the basis of the beginning of the rise or fall in activity, which was synchronous in cell bodies and axons (Figure S2B). Both ON and OFF states varied greatly in duration, with lengths that ranged from a few seconds to several minutes in animals held in constant conditions (Figure S2C).

Correlated activity among a set of neurons that includes AIB and AVA has also been observed in whole-brain imaging (Schröder et al., 2013; Prevedel et al., 2014), in agreement with these observations. To assess the degree of correlation between the interneurons, AIB, RIM, and AVA were simultaneously imaged and then independently classified into ON or OFF states for animals imaged for 1 min in buffer (Figures S2 and S3). Most neuronal state transitions were correlated to within a few seconds, which is at the limit of resolution of the binary classification scheme. AVA produced the clearest transitions between ON and OFF states, whereas the slower calcium dynamics of RIM led to less precise transition assignments. AIB had relatively fast calcium dynamics and also displayed more low-amplitude high frequency (second, subsecond) dynamics in the ON state that made shorter ON/OFF assignments less precise (Figures 2A and 2C; Figure S3).

Of the eight possible binary states of AIB, RIM, and AVA, only three occurred for time frames longer than 10 s: (1) all neurons ON, (2) all neurons OFF, or (3) AIB only (AIB-ON, AVA/RIM-OFF) (Figure 2E; Figure S2D). The AIB-only state could last for many seconds when it did occur (Figure S2D). Mutual information analysis confirmed that AVA and RIM are more tightly coupled to one another than to AIB (Experimental Procedures; Figure S3). Transitions between the three network states continued over several hours in animals that were physically immobilized in the absence of externally applied sensory stimuli or pharmacological agents.

### Odor Addition Drives State Transitions in AIB, RIM, and AVA Interneurons

IAA addition induces a rapid and reliable suppression of activity in AWC sensory neurons (Figure 1D; Chalasani et al., 2007). Odor effects on interneurons were more variable and were most easily understood in the context of the distinct ON and OFF network states.

We first considered each interneuron independently. The average intermediate response to odor addition (Figure 1D) resulted from some neurons that responded very strongly soon after odor addition and others that did not respond at all. This effect was most evident when neuronal activity profiles were binned according to their state just prior to odor addition and sorted on the basis of the time to the next transition (Figure 3A). A majority of the AIB, RIM, and AVA neurons in the ON state responded to odor with a transition to the OFF state within a few seconds, and a minority did not. Neurons in the OFF state remained OFF after odor addition, presumably because they could not be suppressed below this apparent baseline. To quantify the

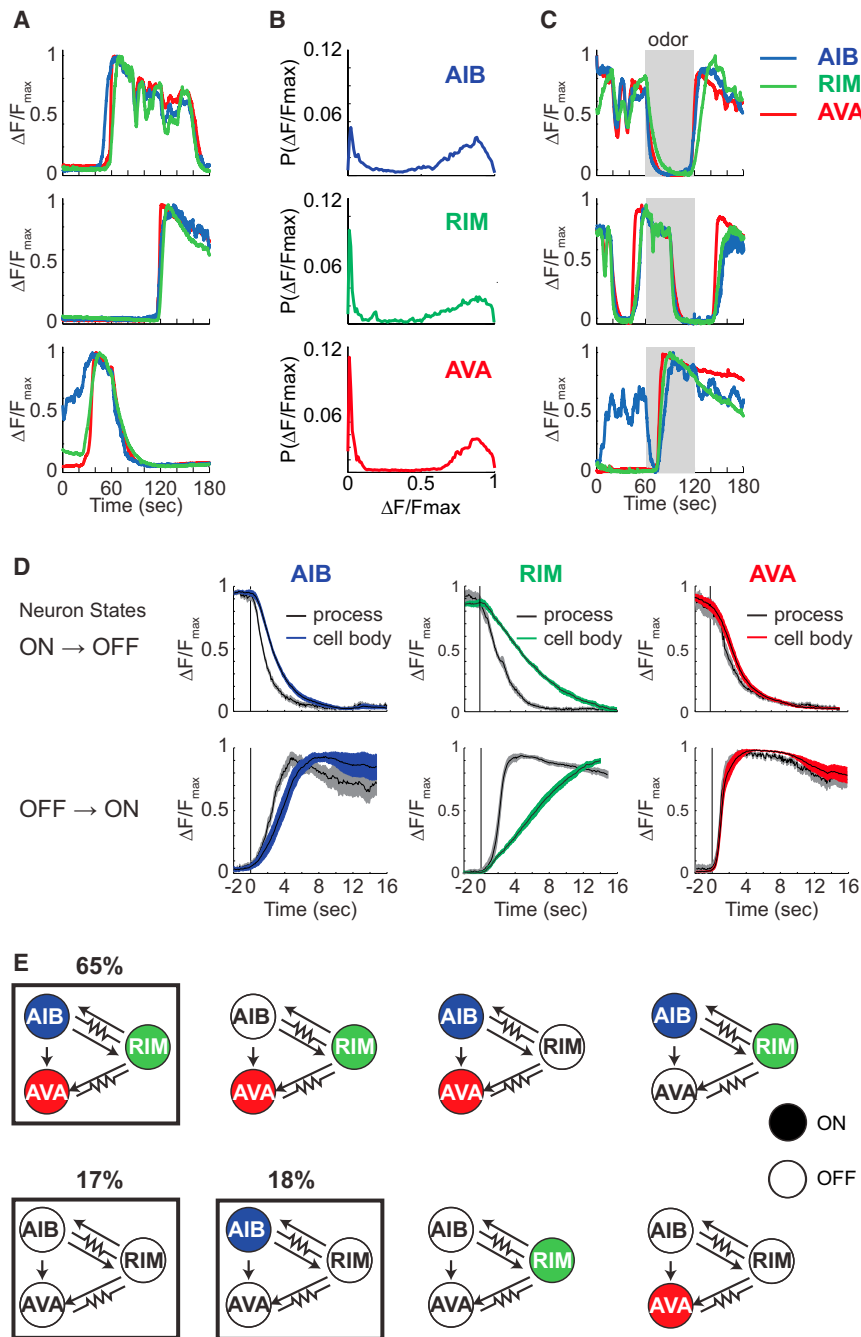


**Figure 2. AIB, RIM, and AVA Have Bistable, Correlated Activity States**

(A) Representative calcium dynamics in simultaneously recorded AIB, RIM, and AVA neurons from three animals in buffer.

(B) Probability distribution of normalized calcium activity showing bimodal distribution of activity in AIB, RIM, and AVA neurons in buffer (n = 83).

(C) Representative calcium dynamics in simultaneously recorded AIB, RIM, and AVA neurons from three animals in response to a 1-min odor pulse (gray bars). Shaded areas are SEM.

(D) Calcium dynamics in simultaneously imaged cell bodies (color) and processes (gray), aligned to ON  $\rightarrow$  OFF and OFF  $\rightarrow$  ON transitions (n = 17). Shaded areas are SEM. Calcium dynamics from individually imaged neurons are normalized to peak and trough values for each trace in all panels.

(E) The eight possible network states and the observed frequencies of each state lasting longer than 10 s during a 1-min period prior to odor exposure (n = 83).

ure S3E). These results suggest that odor drives collective all-or-none transitions in multiple interneurons to shift network states.

Odor addition had other effects on interneuron activity as well (Figures 3D–3H). For all three interneurons, the median duration of the initial OFF response induced by odor was 5- to 10-fold longer than in buffer controls (Figure 3E; Figure S2C), and the total fraction of time spent in the ON state decreased 2- to 4-fold (Figure 3F). In addition to large-scale ON-OFF transitions, odor often elicited a rapid, small-amplitude decrease in the calcium signal of the AIB neuron, which was not always accompanied by a full OFF state or by similar changes in the RIM and AVA neurons (Figures 3G and 3H; Figures S3C and S3D).

The odor-regulated, inefficient, all-or-none transitions in neuronal activity of AIB, RIM, and AVA seemed of particular interest for probabilistic reversal behavior: they captured both the delay and the variability characteristic of the behavioral

effect of odor addition, we measured the time after odor exposure at which each interneuron switched from an ON to OFF state and compared with controls switched from buffer to buffer (Figures 3B–3D). Odor shifted the entire distribution of AIB, RIM, and AVA neurons toward OFF states within a few seconds, an effect that was strongest for AIB.

The responses of simultaneously imaged AIB, RIM, and AVA neurons to odor addition were highly correlated with one another; in most cases, either all three neurons shifted from an ON to an OFF state at similar times or none did (Figure 1D; Fig-

output (Larsch et al., 2013). These transitions transform reliable AWC activity into variable AVA responses.

**RIM Neurons Create Variability in AIB Odor Responses**

An insight into the source of interneuron variability was provided by the network state in which only AIB was ON. In AIB-only states, unlike all-ON states, odor addition always drove a transition to the all-OFF state (Figures 3I and 3J). This class of events largely explained the higher fraction of odor response in AIB neurons compared with RIM and AVA. Moreover, the AIB-only

neurons responded more rapidly to odor than AIB neurons in an all-ON state (Figure 3K). The rapid and reliable AIB-only response to odor indicates that a network property correlated with RIM and AVA activity antagonizes the AIB odor response.

To explore the functional importance of the AIB-only network state, we manipulated neuronal activity with a chemogenetic reagent, the histamine-gated chloride channel HisCl1. *C. elegans* does not use histamine as an endogenous neurotransmitter, but *C. elegans* neurons that express *Drosophila* HisCl1 are acutely hyperpolarized within a few minutes of exposure to exogenous histamine (Pokala et al., 2014). This reagent enabled the silencing of specific neurons under conditions compatible with neuronal activity imaging. HisCl1 was individually expressed in AIB, RIM, or AVA neurons, or in pairwise combinations of these neurons, to generate histamine-sensitive strains. These strains also expressed GCaMP3 in AIB, RIM, and AVA.

Acute silencing of both AVA and RIM eliminated their calcium transients, recapitulating the AIB-only state (Figure 4A). In animals in which RIM and AVA were acutely silenced with histamine, odor addition shifted AIB neurons from the ON to the OFF state with high reliability and a significantly shorter latency than controls (Figures 4B, fifth row, 4C, and 4D). A similar effect was observed when RIM and AVA were removed from the circuit using an *nmr-1::ICE* transgene that results in programmed cell death of RIM, AVA, and four other neuron classes (Zheng et al., 1999). AIB neurons in *nmr-1::ICE* animals responded rapidly and reliably to odor addition (Figure S4), resembling wild-type animals in the AIB-only state. Thus, the activity of RIM and AVA neurons delays and diminishes odor responses in AIB.

In addition to imitating endogenous network states, the cell-specific HisCl1 transgenes made it possible to generate alternative network states. Thus, with appropriate transgenes it was possible to silence only AVA or only RIM with HisCl1, although these states were not normally observed. Silencing either RIM or AVA decreased the latency and increased the efficiency of AIB odor responses, with RIM having a stronger effect (Figures 4B, third and fourth rows, 4C, and 4D). These results indicate that AIB interneurons are subject to feedback from RIM and AVA neurons and that this feedback is one source of variability in the AIB odor response.

### Interactions between AIB, RIM, and AVA Shape Odor Responses and Network States

In the All-ON state, AIB, RIM, and AVA interneurons respond to odors after a variable delay, if at all. Using HisCl silencing, we probed the effect of each of these three neurons on the odor responses of the others, alone and in combination.

Silencing either RIM or AVA increased the speed and reliability of the odor response in AVA or RIM, respectively, as well as AIB (Figures 4B–4D). Thus, RIM and AVA can each act independently to antagonize odor responses.

Silencing AIB had little effect on the onset of odor responses in RIM and AVA (Figures 4C and 4D), indicating that other inputs such as the direct AWC to AVA synapses are sufficient to drive odor responses. However, silencing AIB considerably decreased the duration of the OFF responses induced by odor in RIM and AVA (Figures 4E and 4F), indicating that AIB stabilizes odor-induced OFF states.

Silencing RIM decreased the correlation of activity between AIB and AVA neurons, suggesting that RIM has a key role in synchronizing network states (Figure 4H). Other interactions in the circuit were suggested by pairwise silencing. For example, simultaneous silencing of AIB and RIM led to a striking reduction in spontaneous AVA activity (Figure 4B, seventh row). This result suggests that both AIB and RIM provide excitatory drive to the backward command system. None of the manipulations of neuronal activity changed the bistable, switchlike behavior of the AIB, RIM, and AVA neurons.

### Chemical Synapses Mediate the Antagonistic Effects of AIB and RIM

AIB and RIM are strongly coupled to one another in the *C. elegans* wiring diagram, with bidirectional chemical synapses as well as gap junctions. RIM and AVA are connected by unidirectional chemical synapses and by gap junctions (Figure 5A). To separate the contributions of chemical synapses and gap junctions, we used cell-specific expression of tetanus toxin light chain from *Clostridium tetani* (TeTx). TeTx reduces presynaptic vesicle release by cleaving synaptobrevin/VAMP, but should spare gap junctions and neuronal excitability (Schiavo et al., 1992).

Expression of TeTx in AIB delayed odor responses in RIM and AVA and substantially decreased the length of their OFF response. Remarkably, AIB:TeTx also delayed odor responses and shortened the initial OFF duration in AIB itself, though the effect was not as strong as in RIM and AVA (Figures 5B–5D). Thus the latency and length of an AIB response to odor depends in part on AIB synaptic output, suggesting that AIB synapses oppose the antagonistic feedback that decreases AIB reliability.

Conversely, expression of TeTx in RIM increased the reliability of AIB and AVA odor responses and decreased their latency, resembling the effects of RIM::HisCl silencing (Figures 5B–5D). RIM::TeTx also increased the reliability of the RIM response to odor. Indeed, silencing RIM chemical synapses with TeTx converted the entire network to a near-deterministic state, with over 80% of the neurons responding to odor addition with a rapid switch from the ON to OFF state that is as fast as the initial AIB response (Figures 5B–5G). These results indicate that RIM chemical synapses antagonize odor input to generate probabilistic behavior in the interneuron network.

AVA does not make chemical synapses onto AIB or RIM, but it has gap junctions with RIM. To probe the role of AVA feedback on the other neurons, we stimulated AVA with the red light-sensitive cation channel Chrimson (Klapoetke et al., 2014) during calcium imaging with GCaMP. Activation of AVA led to simultaneous calcium increase in AVA, RIM, and AIB (Figure 5H), demonstrating that feedback from AVA is sufficient to drive AIB and RIM into high-activity states.

### RIM Decreases the Reliability of Behavioral Responses to Odors

Although calcium imaging in restrained animals permitted simultaneous imaging of multiple neurons, it precluded analysis of the behaviors triggered by odor. To characterize the relationships between neuronal activity and behavior, we monitored the activity of individual interneurons in freely moving animals, using microfluidic arenas suitable for fast switching of odor stimuli

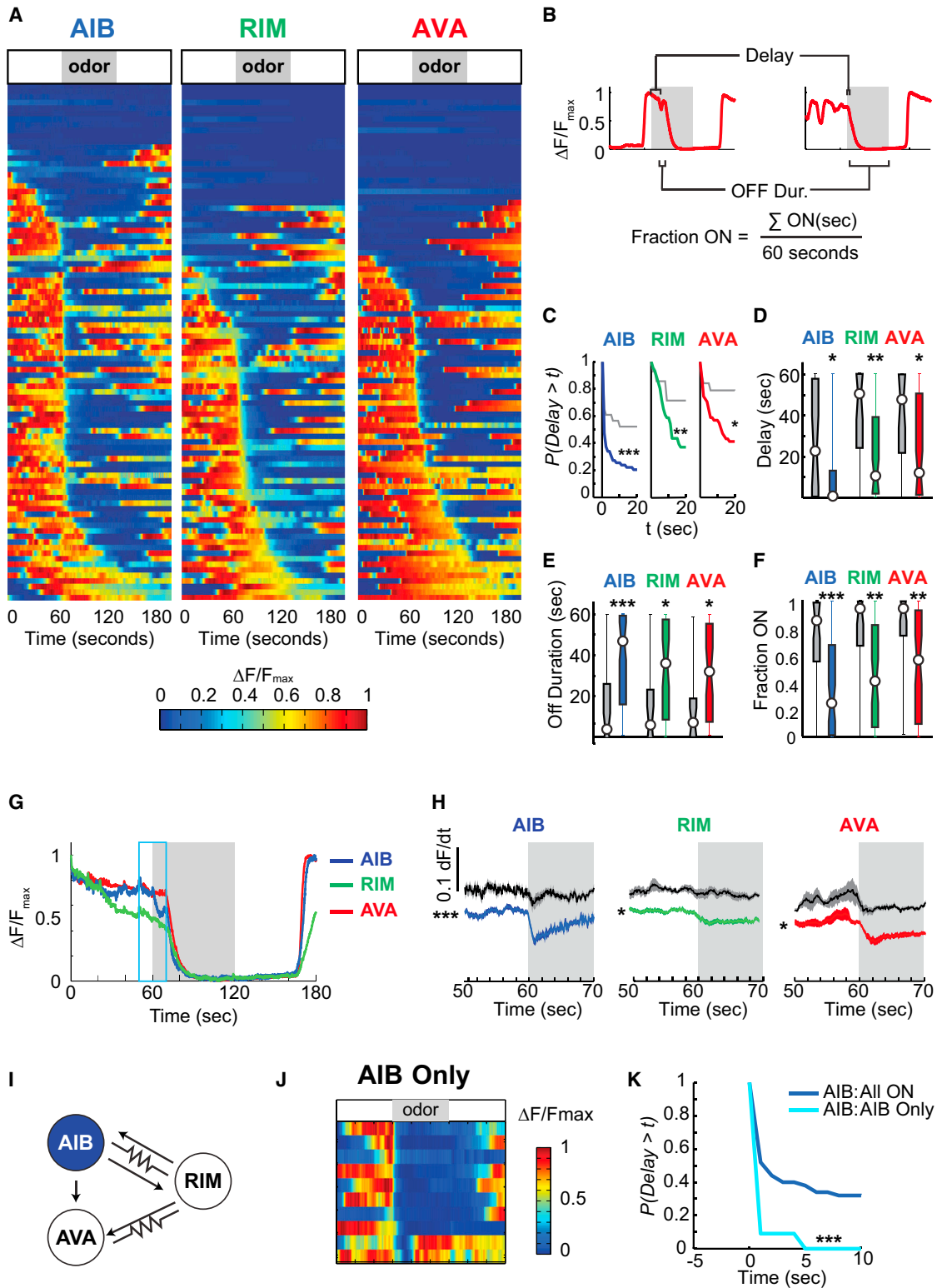


**Figure 3. AIB, RIM, and AVA Calcium Is Reduced by Odor Addition**

(A) Calcium dynamics in simultaneously recorded AIB, RIM, and AVA neurons. Traces from Figure 1D are ordered separately for each neuron according to its activity at the point of odor addition (gray bar above heatmaps) and secondarily according to the closest ON to OFF transition for that neuron. Buffer control data are in Figure S3.

(legend continued on next page)

(Larsch et al., 2013) (Figure 6A). GCaMP-expressing animals were exposed to repeated odor pulses or buffer while recording both the responses of individual interneurons and the behavior of the animal. As shown previously, AWC activity was reliably modulated by odor addition and removal (Figure 6B). On average, the activity of AIB, RIM, and AVA also fell when odor was added and rose when odor was removed, as it did in restrained animals (Figure 6B).

Alignment of neuronal activity with behavioral status of the animals showed that the activity of all three interneurons was also correlated with reversal behaviors, whether these were spontaneous (Figure 6C) or induced by odor (Figure S5). This correlation was not observed for AWC unless odor stimuli were used. The beginning of a reversal coincided with rising AIB, RIM, or AVA calcium, and the end of the reversal corresponded to falling calcium. These results suggest that the activity of AIB, RIM, and AVA is correlated in freely moving as well as restrained animals and indicate that the all-ON state corresponds to reversals. Nonetheless, there were differences in the calcium dynamics of restrained and freely moving animals; high-activity ON states were shorter in freely moving animals, as has previously been noted for AVA (Chronis et al., 2007; Ben Arous et al., 2010; Faumont et al., 2011).

Since RIM decreased the reliability of odor responses in AIB, RIM, and AVA, it should affect the corresponding behavioral responses to odor. To test this prediction, RIM synapses were inactivated with TeTx synaptic silencing, and odor pulses were delivered under conditions that led to probabilistic reversal responses (Figure 6D). As predicted by the imaging experiments, RIM:TeTx animals had a more reliable response to odor addition than wild-type animals (Figure 6D). Thus, behavioral variability in the odor response, like neuronal variability, is increased by RIM.

## DISCUSSION

Animals navigating a complex environment do not simply reproduce external stimuli through their actions; instead, they shape behavior appropriate to conditions. Chemotaxis circuits can transform smooth or noisy sensory inputs into discrete, probabilistic reorientations. More generally, animals make choices and explore environments through discrete, mutually exclusive actions, which are also the basis of experimental behavioral paradigms such as go-nogo or forced choice decisions (Frederick

et al., 2011). Here we consider one question raised by this class of behavior: how are such probabilities resolved into decisions?

Although sensory information can be limiting for performance, sensory noise in the *C. elegans* chemotaxis circuit is not the source of probabilistic behavior. AWC responds to odor rapidly and reliably in each trial, but at a behavioral level, reorientation behavior is probabilistic at odor concentrations 1,000-fold higher than the detection threshold (Larsch et al., 2013). Instead, our results indicate that interneurons integrate the sensory response with ongoing network activity to generate responses that vary in their timing and probability.

The AIB interneurons are major synaptic targets of AWC and are also direct or indirect targets of many other sensory neurons (Figure 7). Although AIB neurons respond to odors more reliably than other interneurons, they do not respond in every trial. However, AIB can respond to odors more consistently when RIM or AVA is silent. Variability in AIB response to odors thus results from interference from neurons closer to the motor response, the backward command neuron AVA and the interneuron RIM. Effectively, sensory input and RIM compete to regulate AIB, which then acts with RIM, AVA, and other neurons in a collective network state.

Both RIM and AIB chemical synapses affect the network. RIM synapses are an essential component of feedback onto AIB, and indeed the RIM connection to AIB is very strong when both synapse size and synapse number are taken into account ([www.wormwiring.org](http://www.wormwiring.org)) (Figure 7). RIM releases the neurotransmitters glutamate, acetylcholine, and tyramine, any of which could potentially act on AIB. AIB's own chemical synapses promote its odor response, potentially by antagonizing feedback from RIM and AVA. AIB uses glutamate as a transmitter, and RIM expresses both excitatory and inhibitory glutamate receptors (Hart et al., 1995; Maricq et al., 1995; Piggott et al., 2011). The detailed properties of these synapses remain to be determined. Another open question is the contribution of the gap junctions linking AIB, RIM, and AVA. Optogenetic activation of AVA can drive the network, and in the context of the wiring diagram this is likely to involve AVA gap junctions with RIM, but these connections do not have well-defined genetics or pharmacology and we did not target them directly. It should be noted that the temporal resolution of calcium imaging is limited, even when using the higher resolution provided by examining axons instead of cell bodies; therefore, this approach reports the final outcome but not the interactions between different chemical synapses and gap junctions.

(B) Example traces highlighting parameters analyzed in (C)–(F). “Delay” is the duration a neuron remained ON after odor addition. “OFF Duration” is the duration of the first OFF response after odor addition. “Fraction ON” is the fraction of time during the 1-min odor pulse that the neuron was ON.

(C–F and H) Analysis of calcium dynamics from (A) for each neuron. In all panels, responses to odors are in color, and buffer controls are in black or gray.

(C) Complementary cumulative distribution (CCD) of the ON → OFF delay for each neuron in response to a 1-min odor (red, green, blue) or buffer (gray) pulse.

(D) Length of the ON → OFF delay after odor addition.

(E) Initial OFF duration after odor addition.

(F) For neurons that were ON prior to odor exposure, the fraction of time the neuron was ON during the 1-min odor pulse. For (D)–(F), box and whisker plots show median response (circle), 25<sup>th</sup> and 75<sup>th</sup> percentile (boxes), and full distribution (lines).

(G) An example trace of AIB briefly responding to odor before a full OFF response. The blue box highlights the time frame in (H).

(H) Staggered mean time derivatives of calcium response for AIB, RIM, and AVA neurons from (A) that were ON prior to odor addition. (Buffer: AIB, n = 23; RIM, n = 24; AVA, n = 19. Odor: AIB, n = 59; RIM, n = 46; AVA, n = 51.) Shaded regions are ±SEM.

(I) Schematic diagram of the “AIB-only” state.

(J) Heatmap of AIB calcium dynamics in response to odor for AIB-only state.

(K) Complementary cumulative distribution (CCD) of the ON → OFF delay after odor addition for the AIB-only state.

p values compared with controls were calculated with a Kolmogorov-Smirnov test (C and K) or Wilcoxon rank sum test with Bonferroni correction (D–F and H). \*p < 0.05, \*\*p < 0.01, \*\*\*p < 0.001.

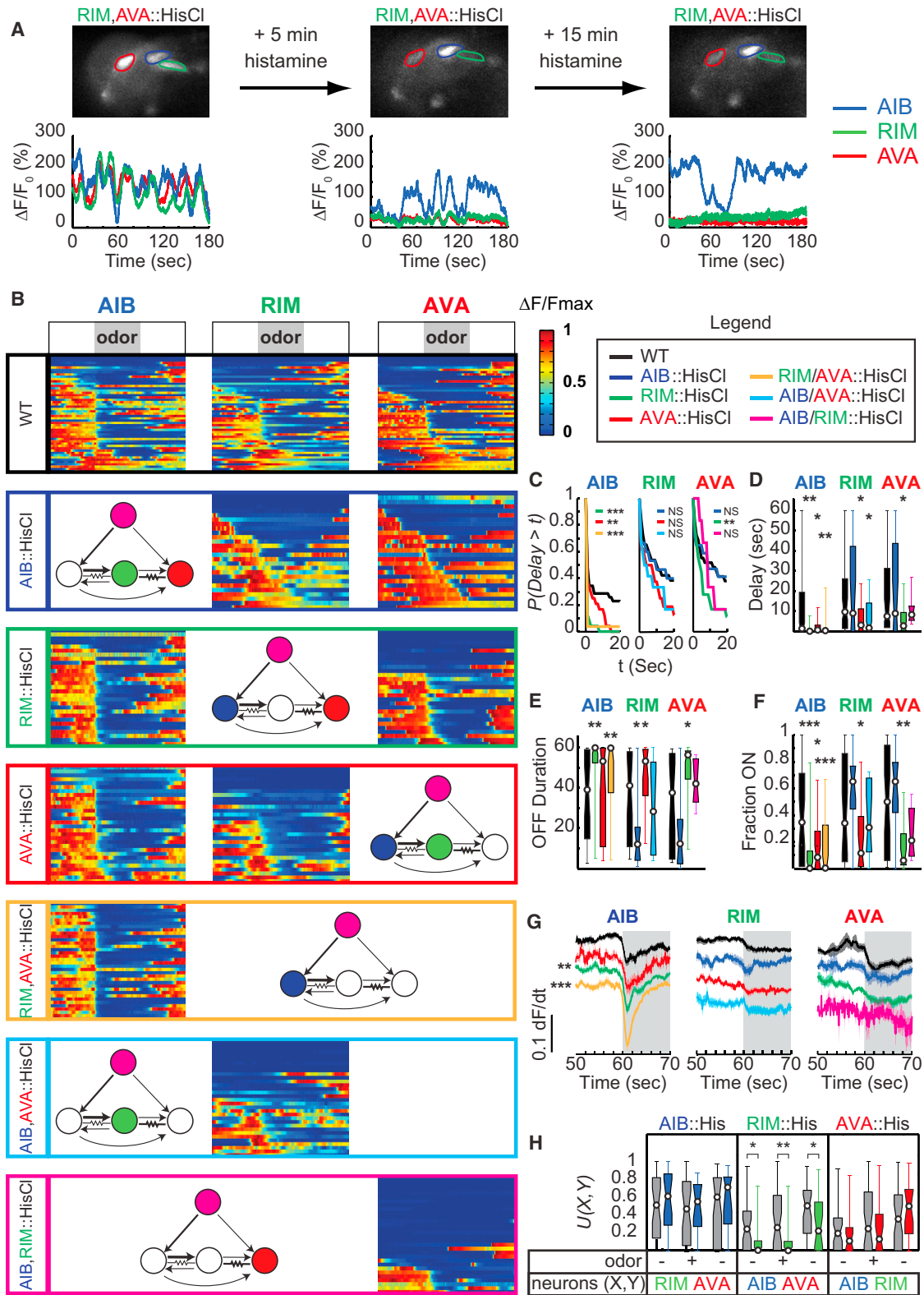


**Figure 4. RIM Hyperpolarization Increases Reliability in AIB and AVA Neurons**

(A) Representative images and traces of spontaneous activity of AIB, RIM, and AVA neurons in animals expressing HisCl1 in RIM and AVA. Left: spontaneous activity in buffer in the absence of histamine. Middle: after exposure to 10 mM histamine for 5 min. Right: after exposure to 10 mM histamine for 20 min.

(legend continued on next page)

The *C. elegans* wiring diagram is dominated by feed-forward connections (White et al., 1986; Varshney et al., 2011), but our results demonstrate a strong feedback component from ongoing network states that evolve on a slow second to minute timescale. This feedback is evident as early as the AIB interneurons, which are generally considered sensory integrators. The faster computations at the sensory level and slower computations in collective network states allow multiple timescales of behavior to emerge. Feedback from slow network states can be envisioned as inertia in the system: once an ON or OFF state is generated, it overrides other inputs that must accumulate or wait for the network state to decay. We speculate that the collective states of AIB, RIM, and AVA represent attractor states, in which different starting points lead to a stable, self-reinforcing activity state that is either high or low (Hopfield, 1982). The factors determining the duration of the network states are unknown. Both ON and OFF states follow exponential distributions, but that leaves open a large number of mechanisms that could be stochastic, chaotic, or simply complex.

The analysis presented here provides a first view of probabilistic behavior, but there are almost certainly other neurons that participate in these decisions (Figure 7). Many other neurons are synaptically connected to AIB, RIM, and AVA and could affect transitions between high and low network states, which in turn could affect additional interacting neurons. For example, AVB, the forward command neuron, receives strong synaptic input from both AIB and RIM and synapses onto AVA; it is likely an element of an antagonistic network. Recent whole-brain imaging studies of *C. elegans* have shown that AVA, AIB, and several dozen other neurons have correlated activities (Schröder et al., 2013; Prevedel et al., 2014). Our results agree with their conclusion that neurons in *C. elegans* have collective activity states, and the whole-brain imaging suggests that many other neurons could contribute to all-ON, all-OFF, and other possible network states.

There is still much to learn about the composition and properties of collective neuronal states, particularly in freely moving animals. Most of our results, as well as the whole-brain imaging of Schröder et al. (2013), were obtained in the presence of a cholinergic agonist that could have altered network activity. Moreover, we and others have observed that neuronal dynamics are altered when animals are physically restrained (Ben Arous et al., 2010), perhaps because of mechanical inputs or a loss of motor and proprioceptive feedback (Kawano et al., 2011).

The importance of network state on sensory processing has long been recognized in mammalian visual cortex and other systems. For example, behavioral detection of visual stimuli by human subjects can be predicted from ongoing network activity, independent of the stimulus (Ress et al., 2000). Selective attention, task-specific information, and motor feedback can affect sensory processing in mammalian visual cortex (Silver et al., 2007; Li et al., 2004; Niell and Stryker, 2010). Motor feedback also affects the gain of visual processing in the fly brain (Maimon et al., 2010).

The integration of sensory information with network states has appealing properties from a behavioral standpoint. First, a fully determined behavior may be appropriate to certain intrinsically meaningful stimuli—highly toxic environmental conditions, food, and suitable mates—but most stimuli do not necessarily produce a predictable outcome and are not themselves rewarding. In that context, variability can prevent behavioral dead ends and increase real success. Second, different behaviors can emerge by changing the underlying state dynamics, as well as sensory properties. For example, *C. elegans* has a much higher probability of spontaneous reversals immediately after removal from food than it has an hour later, presumably accompanied by differences in AVA and RIM activity, which would lead to differences in the transmission of sensory information from AWC to AIB (Gray et al., 2005). Sensory cues that are integrated with circuit state could accordingly generate different behaviors under different feeding states. Third, adjusting the strength of different inputs in a probabilistic network increases opportunities for plasticity, and indeed AIB and RIM participate in *C. elegans* learning circuits (Ha et al., 2010). Further investigation of the generation and control of variability may provide additional insight into these more complex behavioral mechanisms.

## EXPERIMENTAL PROCEDURES

Standard culture, molecular biology, injection, and optogenetic methods were used; details and strain genotypes are in Extended Experimental Procedures. For GCaMP and HisCl expression, we used promoters for *rig-3* (expressed in AVA and some pharyngeal neurons), *tdc-1* (RIM and RIC), *inx-1* (AIB), and *str-2* ( $AWC^{ON}$ ). For ChR2 or Chrimson expression, we used the same promoters except for AVA, for which we used Cre/Lox recombination and the intersection between *nmr-1* and *rig-3* promoters (ChR2) and *glr-1* and *rig-3* promoters (Chrimson).

(B) Heatmaps of calcium dynamics in AIB, RIM, and AVA neurons (columns) in different HisCl-expressing strains (rows) during exposure to a 1-min pulse of 92  $\mu$ M IAA (gray bars) in the presence of histamine. Traces span 3 min and are ordered as in Figure 3A. Neuron diagrams are colored as in Figure 1A, with the histamine-silenced neurons shown in white (wild-type [WT],  $n = 51$ ; *AIB::HisCl*,  $n = 27$ ; *RIM::HisCl*,  $n = 29$ ; *AVA::HisCl*,  $n = 30$ ; *RIM,AVA::HisCl*,  $n = 36$ ; *AIB,AVA::HisCl*,  $n = 32$ ; *AIB,RIM::HisCl*,  $n = 30$ ).

(C–G) Analysis of calcium dynamics from data in (B), as in Figure 3. Color legend designates different HisCl strains. (C) Complementary cumulative distribution (CCD) of the ON  $\rightarrow$  OFF delay for each neuron in response to a 1-min odor pulse. (D) Length of the ON  $\rightarrow$  OFF delay after odor addition. (E) Initial OFF duration after odor addition. (F) For neurons that were ON prior to odor addition, the fraction of time the neuron was ON during the 1-min odor pulse. For (D)–(F) and (H), box and whisker plots show median response (circles), 25<sup>th</sup> and 75<sup>th</sup> percentile (boxes), and full distribution (lines). (G) Staggered mean time derivatives of calcium response for AIB, RIM, and AVA neurons that were ON prior to odor addition under different histamine-silenced conditions. Shaded regions are  $\pm$ SEM.

(H) Symmetric uncertainty coefficient for neuron pairs after silencing AIB, RIM, or AVA with HisCl (see Statistical Methods). A coefficient of one means both neurons are mutually dependent, while a coefficient of zero means they are completely independent. Gray indicates control values without hyperpolarization. Note that RIM and AVA are more tightly coupled to one another than to AIB. Silencing RIM significantly decreases the mutual information between AIB and AVA neurons.

p values compared with WT controls were calculated with a Kolmogorov-Smirnov test (C) or Wilcoxon rank sum test with Bonferroni correction (D–H). \* $p < 0.05$ , \*\* $p < 0.01$ , \*\*\* $p < 0.001$ .

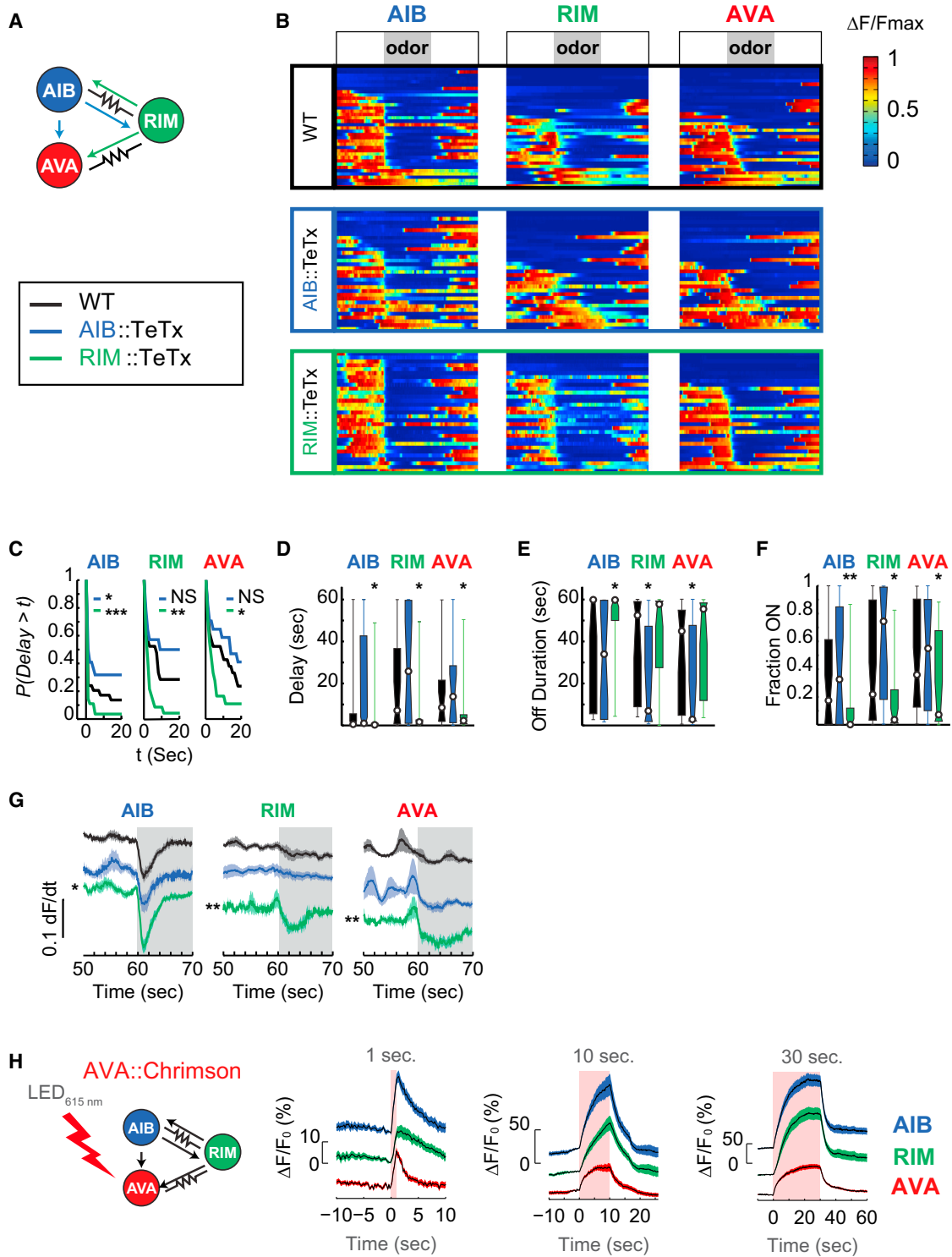


**Figure 5. RIM Chemical Synapses Drive Variability in Odor Responses**

(A) Schematic showing synapses affected by tetanus toxin expression.

(B) Heatmap of calcium dynamics in AIB, RIM, and AVA neurons (columns) in different tetanus toxin-expressing strains (rows) during exposure to a 1-min pulse of 92  $\mu$ M IAA (gray bars). Traces span 3 min and are ordered as in Figure 3A. (WT, n = 37; AIB::TeTx, n = 32; RIM::TeTx, n = 31).

(C–G) Analysis of calcium dynamics from data in (B), as in Figure 3. Color legend in (A) designates TeTx-expressing strains. (C) Complementary cumulative distribution (CCD) of the ON  $\rightarrow$  OFF delay for each neuron in response to a 1-min odor pulse. (D) Length of the ON  $\rightarrow$  OFF delay after odor addition. (E) Initial OFF

(legend continued on next page)

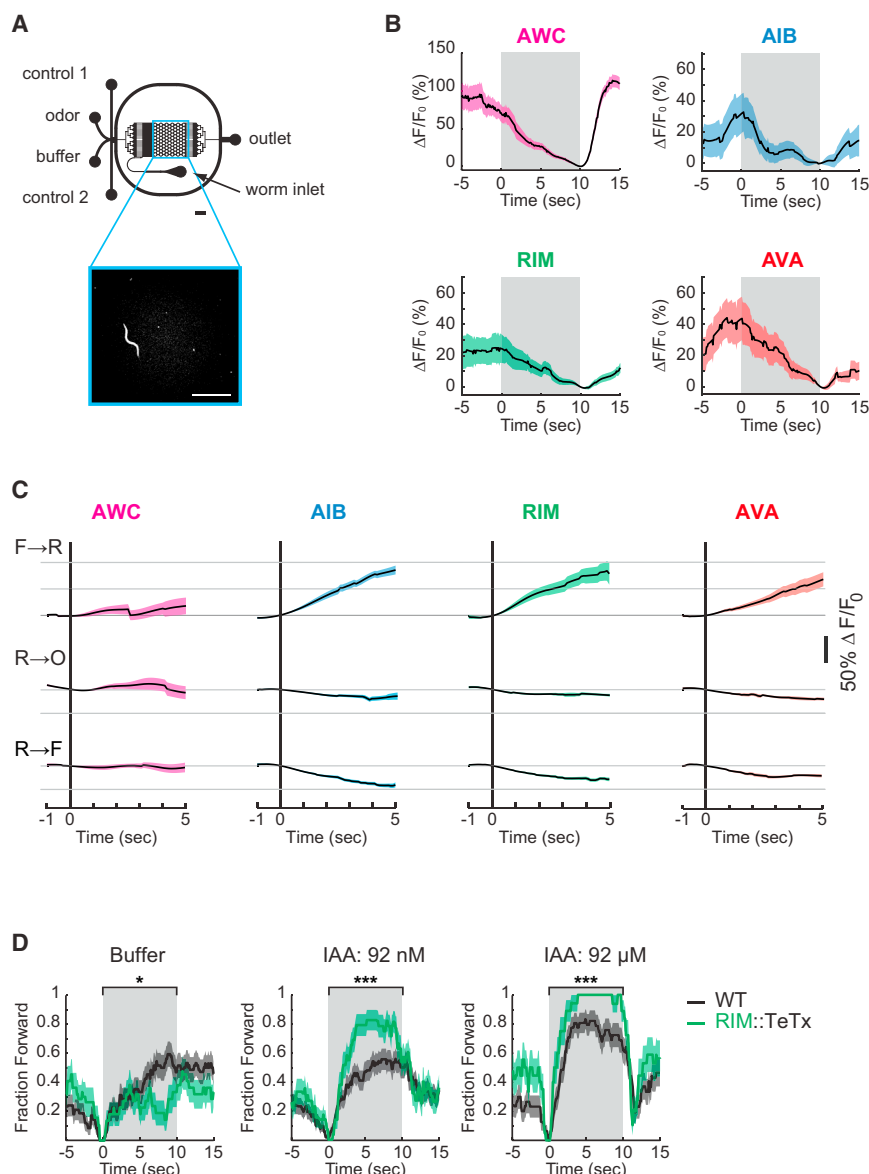


**Figure 6. Activity of AIB, RIM, and AVA Correlates with Reversals in Freely Moving Animals**

(A) Schematic of microfluidic arena used to record calcium dynamics in freely moving animals. Animals were loaded via the worm inlet. The flow of odor or buffer into the arena was controlled by positive flow from control inlets 1 and 2, respectively. Scale bars, 1 mm.

(B) Mean neuronal calcium responses during a 10-s exposure to 92  $\mu\text{M}$  IAA (gray bar). Note different y axis for AWC and interneurons. Eight repeated 10-s exposures per animal; number of animals: AWC,  $n = 6$ ; AIB,  $n = 4$ ; RIM,  $n = 4$ ; AVA,  $n = 4$ . Shaded regions are  $\pm\text{SEM}$ .

(C) Mean neuronal calcium responses in buffer aligned to transitions between forward, reversal, and omega behaviors. Data normalized to fluorescence at point of transition ( $F_0$ ). Note common y axis for all neurons. (Forward-reversal events: AWC,  $n = 13$ ; AIB,  $n = 25$ ; RIM,  $n = 20$ ; AVA,  $n = 23$ . Reversal-omega events: AWC,  $n = 14$ ; AIB,  $n = 10$ ; RIM,  $n = 24$ ; AVA,  $n = 16$ . Reversal-forward events: AWC,  $n = 21$ ; AIB,  $n = 33$ ; RIM,  $n = 40$ ; AVA,  $n = 20$ .) Shaded regions are  $\pm\text{SEM}$ .

(D) Behavioral responses of wild-type or RIM:TeTx animals exposed to 10 s of buffer, 92 nM IAA, or 92  $\mu\text{M}$  IAA (gray bars). To match calcium imaging data, analysis included only animals showing reversals or other aversive behavior at  $t = 0$  prior to odor addition. Shaded regions are  $\pm\text{SD}$  calculated by 10,000 sampled bootstrap sampling.  $p$  values were calculated with a Kolmogorov-Smirnov test. \* $p < 0.05$ , \*\*\* $p < 0.001$ .

(Andor iXon3 camera, Metamorph Software). In Figures 4 and 5, wild-type data were collected in parallel with genetically modified strains. Data analysis is described in Extended Experimental Procedures.

In a control dataset, the activity of AIB, RIM, and AVA was also imaged in the absence of tetramisole, although the neurons could not be imaged simultaneously due to animal movement. AIB, RIM, and AVA neurons generated spontaneous stochastic bistable activity and responded to odor probabilistically, both in the absence and presence of tetramisole (Figure S5). The immediate responses to odor addition were comparable with or without tetramisole, but the duration of the OFF response was shorter in the absence of tetramisole (Figure S5). The activity of AIB, RIM, and AVA neurons either in buffer or in odor was higher in the absence of tetramisole, i.e., the network was more often in the ON state.

#### Simultaneous Behavioral and Calcium Imaging

Methods followed those described previously (Larsch et al., 2013), using animals in a custom-fabricated  $3 \times 3$  mm polydimethylsiloxane (PDMS) imaging arena with fluid flowing through the arena by gravity flow (210-cm height

#### Calcium Imaging in Restrained Animals

Animals were imaged in custom-built microfluidic chambers (Chronis et al., 2007) in S basal buffer (Brenner, 1974) and paralyzed with 10 mM tetramisole hydrochloride (Sigma-Aldrich) during data acquisition to reduce movement. Each animal was imaged twice, separated by a 5-min interval. For the HisCl1-silencing experiments, 10 mM histamine (Sigma-Aldrich) was included in the pre-incubation starvation conditions, the loading buffer, control buffer, and odor solutions. All animals were starved for 20 min before loading into the chip. Fluid streams were switched using a three-way valve (Lee Company). TIFF stacks were generated at 10 frames per second (fps) using a 40 $\times$  objective

duration after odor addition. (F) For neurons that were ON prior to odor addition, the fraction of time the neuron was ON during the 1-min odor pulse. For (D)–(F), box plots show median response (circles), 25<sup>th</sup> and 75<sup>th</sup> percentile (boxes), and full distribution (lines). (G) Staggered mean time derivatives of calcium response for AIB, RIM, and AVA neurons that were ON prior to odor addition in different tetanus toxin strains.

(H) Calcium dynamics of AIB, RIM, and AVA following optogenetic stimulation of AVA by Chrimson for 1 s, 10 s, and 30 s ( $n = 28$ ). Light pulses ( $\lambda = 615$  nm) are represented by pink bar in all three panels.

Shaded regions are  $\pm\text{SEM}$ .  $p$  values compared with WT controls were calculated with a Kolmogorov-Smirnov test (C) or Wilcoxon rank sum test with Bonferroni correction (D–G). \* $p < 0.05$ , \*\* $p < 0.01$ , \*\*\* $p < 0.001$ .

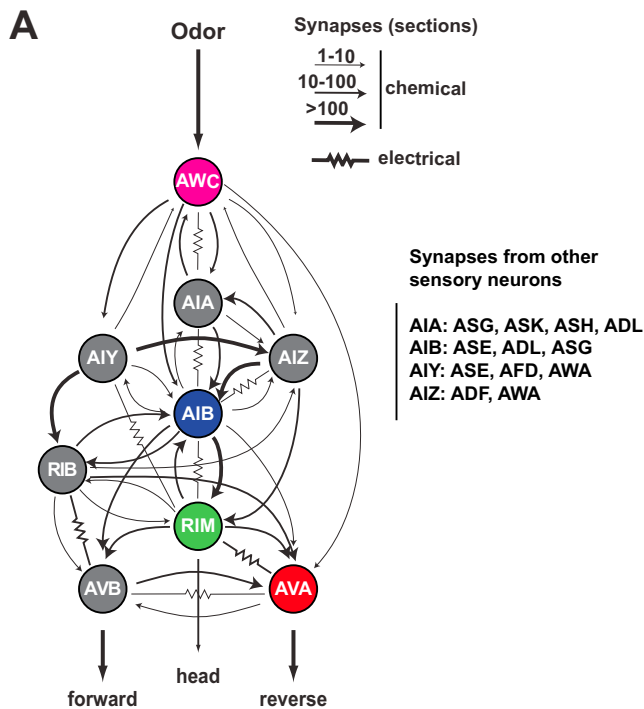


**Figure 7. Weighted Wiring Diagram for AWC, AIB, RIM, and AVA**

(A) Synaptic map of AWC, AIB, RIM, and AVA and other strongly interconnected neurons; arrows were weighted on the basis of the total number of electron micrograph sections in which any synapse was observed (incorporates synapse size and number). Data are from [www.wormwiring.org](http://www.wormwiring.org).

differential, 15 mm/s). Each recording consisted of eight odor pulse sequences separated by 2 min of buffer exposure. Each pulse sequence lasted for 70 s, with alternate 10 s odor, 10 s buffer repeats. The first two of the eight sequences consisted of buffer-to-buffer pulses, followed by two sequences of 92 nM IAA pulses, followed by two sequences of 92  $\mu$ M IAA pulses, followed by two additional buffer-to-buffer pulses. Animals were starved in the arena for 20 min prior to data acquisition.

Metamorph software controlled the camera, light source (Lumencor SOLA-LE solid-state lamp), stimulus delivery (Automate Valvebank 8 II actuator and Lee solenoid valves), and stimulus switching (Hamilton MVP eight-way distribution valve). Stimulus switching occurred during the 2-min buffer exposure when the odor stream was bypassing the arena. TIFF images were collected at 2.5 $\times$  magnification (Hamamatsu Orca Flash 4 cMOS, Metamorph software) at 10 fps with 10-ms pulsed illumination for each 100-ms frame. Neuronal fluorescence just prior to odor removal ( $F_0$ ) was used to calculate the  $\Delta F/F_0$  for the odor-aligned fluorescence data in Figure 6B. Behaviors were binned into forward, reversal, pause and omega states, and manually corrected to ensure accuracy of the timing of transitions between states. For Figure 6C, only fluorescent data from behaviors that spanned the full observational window ( $-1$  to 5 s) were used to calculate the average.

#### Statistical Methods

Since the distribution of most data were not normally distributed based on the Shapiro-Wilk test, the significance of median differences was calculated using the Wilcoxon rank sum test with Bonferroni correction. The Kolmogorov-Smirnov test was used for comparing probability distributions. The systematic uncertainty coefficient for neuron pairs (Figure 4H) was calculated as  $(U(X, Y) = 2 [(H(X) + H(Y) - H(X, Y)) / (H(X) + H(Y))])$  (Press et al., 2002). X and Y represent the binary data for neurons X and Y,  $H(X)$  and  $H(Y)$  are the marginal entropies for X and Y, and  $H(X, Y)$  is the joint entropy for X and Y. The numerator is the mutual information for X and Y, and the denominator is the total entropy. A coefficient

of one means both neurons are mutually dependent, while a coefficient of zero means they are completely independent.

#### SUPPLEMENTAL INFORMATION

Supplemental Information includes Supplemental Experimental Procedures and five figures and can be found with this article online at <http://dx.doi.org/10.1016/j.cell.2015.02.018>.

#### AUTHOR CONTRIBUTIONS

A.G. and C.I.B. designed research; A.G. performed imaging and behavior experiments; N.P. performed optogenetic-behavior experiments; S.L. wrote tracking software for image analysis; S.W.F. developed Chrimson protocols; A.G. and C.I.B. analyzed data; and A.G. and C.I.B. wrote the paper.

#### ACKNOWLEDGMENTS

We thank L. Looger for GCaMP constructs, D. Albrecht and J. Larsch for advice with arena imaging, and S. Kato, M. Lockard, D. Ventimiglia, and other members of our laboratory for helpful discussions. This work was supported by a Marie-Josée and Henry Kravis Postdoctoral Fellowship to A.G., a Human Frontiers Science Program Fellowship to S.L., the G. Harold and Leila Y. Mathers Charitable Foundation, and the Howard Hughes Medical Institute. C.I.B. is a Howard Hughes Medical Institute investigator.

Received: October 20, 2014

Revised: January 9, 2015

Accepted: January 30, 2015

Published: March 12, 2015

#### REFERENCES

- Albrecht, D.R., and Bargmann, C.I. (2011). High-content behavioral analysis of *Caenorhabditis elegans* in precise spatiotemporal chemical environments. *Nat. Methods* 8, 599–605.
- Barlow, H.B., Levick, W.R., and Yoon, M. (1971). Responses to single quanta of light in retinal ganglion cells of the cat. *Vision Res.* 11 (Suppl 3), 87–101.
- Ben Arous, J., Tanizawa, Y., Rabinowitch, I., Chatenay, D., and Schafer, W.R. (2010). Automated imaging of neuronal activity in freely behaving *Caenorhabditis elegans*. *J. Neurosci. Methods* 187, 229–234.
- Benzi, R., Sutera, A., and Vulpiani, A. (1981). The mechanism of stochastic resonance. *J. Phys. A Math. Gen.* 14, L453–L457.
- Berg, H.C., and Brown, D.A. (1972). Chemotaxis in *Escherichia coli* analysed by three-dimensional tracking. *Nature* 239, 500–504.
- Bialek, W. (1987). Physical limits to sensation and perception. *Annu. Rev. Biophys. Chem.* 16, 455–478.
- Brenner, S. (1974). The genetics of *Caenorhabditis elegans*. *Genetics* 77, 71–94.
- Chaisanguanthum, K.S., Shen, H.H., and Sabes, P.N. (2014). Motor variability arises from a slow random walk in neural state. *J. Neurosci.* 34, 12071–12080.
- Chalasan, S.H., Chronis, N., Tsunozaki, M., Gray, J.M., Ramot, D., Goodman, M.B., and Bargmann, C.I. (2007). Dissecting a circuit for olfactory behaviour in *Caenorhabditis elegans*. *Nature* 450, 63–70.
- Chalfie, M., Sulston, J.E., White, J.G., Southgate, E., Thomson, J.N., and Brenner, S. (1985). The neural circuit for touch sensitivity in *Caenorhabditis elegans*. *J. Neurosci.* 5, 956–964.
- Charnov, E.L. (1976). Optimal foraging, the marginal value theorem. *Theor. Popul. Biol.* 9, 129–136.
- Chronis, N., Zimmer, M., and Bargmann, C.I. (2007). Microfluidics for in vivo imaging of neuronal and behavioral activity in *Caenorhabditis elegans*. *Nat. Methods* 4, 727–731.
- Clark, D.A., Gabel, C.V., Gabel, H., and Samuel, A.D. (2007). Temporal activity patterns in thermosensory neurons of freely moving *Caenorhabditis elegans* encode spatial thermal gradients. *J. Neurosci.* 27, 6083–6090.

- Faumont, S., Rondeau, G., Thiele, T.R., Lawton, K.J., McCormick, K.E., Sottile, M., Griesbeck, O., Heckscher, E.S., Roberts, W.M., Doe, C.Q., and Lockery, S.R. (2011). An image-free opto-mechanical system for creating virtual environments and imaging neuronal activity in freely moving *Caenorhabditis elegans*. *PLoS ONE* 6, e24666.
- Frederick, D.E., Rojas-Libano, D., Scott, M., and Kay, L.M. (2011). Rat behavior in go/no-go, and two-alternative choice odor discrimination: differences and similarities. *Behav. Neurosci.* 125, 588–603.
- Goodman, M.B., Hall, D.H., Avery, L., and Lockery, S.R. (1998). Active currents regulate sensitivity and dynamic range in *C. elegans* neurons. *Neuron* 20, 763–772.
- Gray, J.M., Hill, J.J., and Bargmann, C.I. (2005). A circuit for navigation in *Caenorhabditis elegans*. *Proc. Natl. Acad. Sci. USA* 102, 3184–3191.
- Guo, Z.V., Hart, A.C., and Ramanathan, S. (2009). Optical interrogation of neural circuits in *Caenorhabditis elegans*. *Nat. Methods* 6, 891–896.
- Ha, H.I., Hendricks, M., Shen, Y., Gabel, C.V., Fang-Yen, C., Qin, Y., Colón-Ramos, D., Shen, K., Samuel, A.D., and Zhang, Y. (2010). Functional organization of a neural network for aversive olfactory learning in *Caenorhabditis elegans*. *Neuron* 68, 1173–1186.
- Harsanyi, J.C. (1973). Games with randomly disturbed payoffs: a new rationale for mixed strategy equilibrium. *Int. J. Game Theory* 2, 1–23.
- Hart, A.C., Sims, S., and Kaplan, J.M. (1995). Synaptic code for sensory modalities revealed by *C. elegans* GLR-1 glutamate receptor. *Nature* 378, 82–85.
- Hendricks, M., Ha, H., Maffey, N., and Zhang, Y. (2012). Compartmentalized calcium dynamics in a *C. elegans* interneuron encode head movement. *Nature* 487, 99–103.
- Hessler, N.A., and Doupe, A.J. (1999). Social context modulates singing-related neural activity in the songbird forebrain. *Nat. Neurosci.* 2, 209–211.
- Hopfield, J.J. (1982). Neural networks and physical systems with emergent collective computational abilities. *Proc. Natl. Acad. Sci. USA* 79, 2554–2558.
- Humphries, N.E., Queiroz, N., Dyer, J.R., Pade, N.G., Musyl, M.K., Schaefer, K.M., Fuller, D.W., Brunnschweiler, J.M., Doyle, T.K., Houghton, J.D., et al. (2010). Environmental context explains Lévy and Brownian movement patterns of marine predators. *Nature* 465, 1066–1069.
- Kawano, T., Po, M.D., Gao, S., Leung, G., Ryu, W.S., and Zhen, M. (2011). An imbalancing act: gap junctions reduce the backward motor circuit activity to bias *C. elegans* for forward locomotion. *Neuron* 72, 572–586.
- Kirkpatrick, S., Gelatt, C.D., Jr., and Vecchi, M.P. (1983). Optimization by simulated annealing. *Science* 220, 671–680.
- Klapoetke, N.C., Murata, Y., Kim, S.S., Pulver, S.R., Birdsey-Benson, A., Cho, Y.K., Morimoto, T.K., Chuong, A.S., Carpenter, E.J., Tian, Z., Wang, J., Xie, Y., Yan, Z., Zhang, Y., Chow, B.Y., Surek, B., Melkonian, M., Jayaraman, V., Constantine-Paton, M., Wong, G.K., and Boyden, E.S. (2014). Independent optical excitation of distinct neural populations. *Nat. Methods* 11, 338–346.
- Larsch, J., Ventimiglia, D., Bargmann, C.I., and Albrecht, D.R. (2013). High-throughput imaging of neuronal activity in *Caenorhabditis elegans*. *Proc. Natl. Acad. Sci. USA* 110, E4266–E4273.
- Li, W., Piëch, V., and Gilbert, C.D. (2004). Perceptual learning and top-down influences in primary visual cortex. *Nat. Neurosci.* 7, 651–657.
- Lillywhite, P.G., and Laughlin, S.B. (1979). Transducer noise in a photoreceptor. *Nature* 277, 569–572.
- Longtin, A., Bulsara, A., and Moss, F. (1991). Time-interval sequences in bistable systems and the noise-induced transmission of information by sensory neurons. *Phys. Rev. Lett.* 67, 656–659.
- Maimon, G., Straw, A.D., and Dickinson, M.H. (2010). Active flight increases the gain of visual motion processing in *Drosophila*. *Nat. Neurosci.* 13, 393–399.
- Maricq, A.V., Peckol, E., Driscoll, M., and Bargmann, C.I. (1995). Mechanosensory signalling in *C. elegans* mediated by the GLR-1 glutamate receptor. *Nature* 378, 78–81.
- Mellem, J.E., Brockie, P.J., Madsen, D.M., and Maricq, A.V. (2008). Action potentials contribute to neuronal signaling in *C. elegans*. *Nat. Neurosci.* 11, 865–867.
- Mitsutake, A., Mori, Y., and Okamoto, Y. (2013). Enhanced sampling algorithms. *Methods Mol. Biol.* 924, 153–195.
- Nagel, G., Brauner, M., Liewald, J.F., Adeishvili, N., Bamberg, E., and Gottschalk, A. (2005). Light activation of channelrhodopsin-2 in excitable cells of *Caenorhabditis elegans* triggers rapid behavioral responses. *Curr. Biol.* 15, 2279–2284.
- Niell, C.M., and Stryker, M.P. (2010). Modulation of visual responses by behavioral state in mouse visual cortex. *Neuron* 65, 472–479.
- Ölveczky, B.P., Andalman, A.S., and Fee, M.S. (2005). Vocal experimentation in the juvenile songbird requires a basal ganglia circuit. *PLoS Biol.* 3, e153.
- Pierce-Shimomura, J.T., Morse, T.M., and Lockery, S.R. (1999). The fundamental role of pirouettes in *Caenorhabditis elegans* chemotaxis. *J. Neurosci.* 19, 9557–9569.
- Piggott, B.J., Liu, J., Feng, Z., Wescott, S.A., and Xu, X.Z.S. (2011). The neural circuits and synaptic mechanisms underlying motor initiation in *C. elegans*. *Cell* 147, 922–933.
- Pokala, N., Liu, Q., Gordus, A., and Bargmann, C.I. (2014). Inducible and titratable silencing of *Caenorhabditis elegans* neurons in vivo with histamine-gated chloride channels. *Proc. Natl. Acad. Sci. USA* 111, 2770–2775.
- Press, W.H., Teukolsky, S.A., Vetterling, W.T., and Flannery, B.P. (2002). Numerical recipes in C++: the art of scientific computing (Cambridge: Cambridge University Press).
- Prevedel, R., Yoon, Y.G., Hoffmann, M., Pak, N., Wetzstein, G., Kato, S., Schrödel, T., Raskar, R., Zimmer, M., Boyden, E.S., and Vaziri, A. (2014). Simultaneous whole-animal 3D imaging of neuronal activity using light-field microscopy. *Nat. Methods* 11, 727–730.
- Rajan, K., Abbott, L.F., and Sompolinsky, H. (2010). Stimulus-dependent suppression of chaos in recurrent neural networks. *Phys. Rev. E Stat. Nonlin. Soft Matter Phys.* 82, 011903.
- Ress, D., Backus, B.T., and Heeger, D.J. (2000). Activity in primary visual cortex predicts performance in a visual detection task. *Nat. Neurosci.* 3, 940–945.
- Schiavo, G., Benfenati, F., Poulain, B., Rossetto, O., Polverino de Lauro, P., DasGupta, B.R., and Montecucco, C. (1992). Tetanus and botulinum-B neurotoxins block neurotransmitter release by proteolytic cleavage of synaptobrevin. *Nature* 359, 832–835.
- Schrödel, T., Prevedel, R., Aumayr, K., Zimmer, M., and Vaziri, A. (2013). Brain-wide 3D imaging of neuronal activity in *Caenorhabditis elegans* with sculpted light. *Nat. Methods* 10, 1013–1020.
- Silver, M.A., Ress, D., and Heeger, D.J. (2007). Neural correlates of sustained spatial attention in human early visual cortex. *J. Neurophysiol.* 97, 229–237.
- Thrun, S. (1992). The role of exploration in learning control. In *Handbook for Intelligent Control: Neural, Fuzzy and Adaptive Approaches*, D.A. White and D.A. Sofge, eds. (Florence, Kentucky: Van Nostrand Reinhold).
- Tian, L., Hires, S.A., Mao, T., Huber, D., Chiappe, M.E., Chalasani, S.H., Petreanu, L., Akerboom, J., McKinney, S.A., Schreiner, E.R., et al. (2009). Imaging neural activity in worms, flies and mice with improved GCaMP calcium indicators. *Nat. Methods* 6, 875–881.
- Tumer, E.C., and Brainard, M.S. (2007). Performance variability enables adaptive plasticity of 'crystallized' adult birdsong. *Nature* 450, 1240–1244.
- Varshney, L.R., Chen, B.L., Paniagua, E., Hall, D.H., and Chklovskii, D.B. (2011). Structural properties of the *Caenorhabditis elegans* neuronal network. *PLoS Comput. Biol.* 7, e1001066.
- White, J.G., Southgate, E., Thomson, J.N., and Brenner, S. (1986). The structure of the nervous system of the nematode *Caenorhabditis elegans*. *Philos. Trans. R. Soc. Lond. B Biol. Sci.* 314, 1–340.
- Zheng, Y., Brockie, P.J., Mellem, J.E., Madsen, D.M., and Maricq, A.V. (1999). Neuronal control of locomotion in *C. elegans* is modified by a dominant mutation in the GLR-1 ionotropic glutamate receptor. *Neuron* 24, 347–361.